

## Electronic spectroscopy of 9,10-dichloroanthracene inside helium droplets

D. Pentlehner and A. Slenczka

Citation: *The Journal of Chemical Physics* **138**, 024313 (2013); doi: 10.1063/1.4773894

View online: <http://dx.doi.org/10.1063/1.4773894>

View Table of Contents: <http://scitation.aip.org/content/aip/journal/jcp/138/2?ver=pdfcov>

Published by the [AIP Publishing](#)

---

### Articles you may be interested in

[Solvatochromism of 9,10-phenanthrenequinone: An electronic and resonance Raman spectroscopic study](#)  
*J. Chem. Phys.* **142**, 024305 (2015); 10.1063/1.4905126

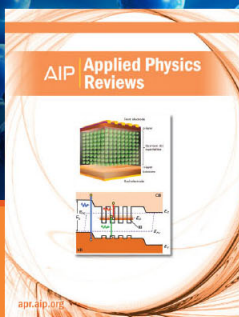
[Infrared-visible and visible-visible double resonance spectroscopy of 1-hydroxy-9,10-anthraquinone-\(H<sub>2</sub>O\)<sub>n</sub> \(n=1,2\) complexes](#)  
*J. Chem. Phys.* **122**, 034305 (2005); 10.1063/1.1829991

[Laser induced fluorescence and resonant two-photon ionization spectroscopy of jet-cooled 1-hydroxy-9,10-anthraquinone](#)  
*J. Chem. Phys.* **122**, 034304 (2005); 10.1063/1.1829977

[Quantum solvation of phthalocyanine in superfluid helium droplets](#)  
*J. Chem. Phys.* **120**, 5064 (2004); 10.1063/1.1647536

[Probing solute-solvent electrostatic interactions: Rotational diffusion studies of 9,10-disubstituted anthracenes](#)  
*J. Chem. Phys.* **106**, 7920 (1997); 10.1063/1.474119

---



**NEW Special Topic Sections**

**NOW ONLINE**  
Lithium Niobate Properties and Applications:  
Reviews of Emerging Trends

**AIP** | Applied Physics  
Reviews

# Electronic spectroscopy of 9,10-dichloroanthracene inside helium droplets

D. Pentlehner<sup>a)</sup> and A. Slenczka<sup>b)</sup>

*Institut für Physikalische und Theoretische Chemie, Universität Regensburg, 93040 Regensburg, Germany*

(Received 21 September 2012; accepted 17 December 2012; published online 10 January 2013)

The spectroscopy of molecules doped into superfluid helium droplets provides information on both, the dopant molecule and the helium environment. Electronic spectra of 9,10-dichloroanthracene in helium droplets are presented and compared with corresponding gas phase spectra to unravel the influence of the helium environment. The combined investigation of fluorescence excitation and dispersed emission provides information on dynamic processes in addition to energetic conditions. For vibronic states, the helium induced decay channels dominate over all intramolecular channels that contribute to the gas phase behavior. In addition to the triplet splitting caused by the Cl isotopes, a fine structure resolved for all transitions in the fluorescence excitation spectrum was found, which is the signature of microsolvation of this compound in helium droplets. This fine structure is identified as a single pure molecular transition accompanied by a sharply structured phonon wing. The corresponding fine structure measured for bare anthracene shows remarkable differences.

© 2013 American Institute of Physics. [<http://dx.doi.org/10.1063/1.4773894>]

## I. INTRODUCTION

Within the last two decades, superfluid helium droplets became a well-established cryogenic matrix for molecular spectroscopy. Several spectroscopic methods were applied to study a large variety of molecular systems embedded in helium droplets including single atoms, molecules, homogeneous and heterogeneous clusters, and unimolecular as well as bimolecular reactions.<sup>1–9</sup>

Among the benefits of using helium droplets as the matrix for these studies are the low temperature of only 0.38 K in combination with a high cooling rate.<sup>2</sup> In case of microwave (MW) and infrared (IR) spectroscopy in helium droplets, the advantages of the superfluid host environment usually outweigh the accompanying perturbations such as solvent shifts or change of rotational constants by far. In particular, line broadening, which is ascribed to inhomogeneous effects or fast relaxation processes, is rather subtle.<sup>10,11</sup> In contrast, numerous examples have been reported showing excessive line broadening in the electronic spectra of molecules when doped into helium droplets.<sup>12,13</sup> In Ref. 13, we discuss changes of the electron density distribution induced by electronic transitions of the dopant molecule to be responsible for line broadening. Thereby, in the case of photon absorption (emission), the density distribution at the ground (excited) state and at the Franck-Condon point of the corresponding molecular excited (ground) state has to be considered. The latter is not necessarily identical with the equilibrium configuration of the electronically excited (ground state) system. Electronic transitions are accompanied by changes of the electron density distribution as reflected by electrostatic moments, and possibly of the intramolecular nuclear configuration, which may per-

turb the droplet environment and finally cause line broadening. This effect differs from what was reported as line broadening for large amplitude modes such as the butterfly mode of pentacene reported by Hartmann *et al.*<sup>14</sup> and confirmed by Callegari and Ernst.<sup>9</sup> Most effective for line broadening appears to be a change of the molecular permanent electric dipole moment, which determines the induction interaction between a neutral molecule and the helium environment. Line broadening in the electronic spectrum of Na dimers in the triplet state, which reside on the surface of the helium droplet,<sup>15</sup> has been explained by a dramatic change of the equilibrium bond length upon electronic excitation causing a softening of the solvation layer.<sup>16</sup> According to the Born-Oppenheimer approximation, we anticipate the redistribution of the electron density distribution to be responsible for a change of the intramolecular nuclear configuration and, similarly, for any perturbation of the helium solvation layer around the dopant molecule. Line broadening is an important phenomenon, which reveals information on electronic excitation, however, masks useful information about the dopant molecule and hides most of the details on the solute-solvent interaction. This interaction is reflected by differences in the (electronic) spectra taken in the gas phase and in helium droplets. Discrepancies between those spectra which cannot be explained by thermal effects include multiplet splitting, phonon wings, or line broadening. Up to now, several details of the underlying interaction are rationalized qualitatively. Quantitative modeling of the spectroscopic features, however, requires continuing experimental and theoretical effort.

The present paper reports on electronic spectroscopy of 9,10-dichloroanthracene (9,10-DCA) doped into superfluid helium droplets. Due to the inversion center, this molecule does not exhibit an electric dipole moment neither in the  $S_0$  ground state, nor in the  $S_1$  electronically excited state. Therefore, in helium droplets line broadening is expected to be rather subtle. The spectroscopy of 9,10-DCA in the gas

<sup>a)</sup>Present address: Department of Chemistry, University of Aarhus, Aarhus, Denmark.

<sup>b)</sup>Author to whom correspondence should be addressed. Electronic mail: [alkwin.slenczka@chemie.uni-regensburg.de](mailto:alkwin.slenczka@chemie.uni-regensburg.de).

phase is well documented in the literature.<sup>17–24</sup> In particular, 9,10-DCA has been investigated in a supersonic jet not only by means of fluorescence excitation, but also via absorption spectroscopy.<sup>20</sup> By comparison of the intensity distribution obtained by the two spectroscopic methods, information on the fluorescence quantum yield and on the non-radiative decay mechanisms was obtained. The combined investigation of the fluorescence excitation spectrum and dispersed emission spectra in comparison with these gas phase data reveals details on the decay mechanism of electronically excited 9,10-DCA in helium droplets. Together with the saturation behavior, excitation and emission spectra allow to assign a helium induced fine structure of each molecular transition to a zero phonon line (ZPL) accompanied by a phonon wing (PW), as demonstrated already for numerous dopant species. As known since long, for solid matrices vibronic excitation is followed by the dissipation of vibrational excess energy into the helium droplet prior to radiative decay.<sup>25–27</sup> The depletion method mainly applied to record the IR spectra of molecules in superfluid helium droplets is based on this mechanism. Finally, the data on 9,10-DCA in helium droplets are an interesting complement to those of bare anthracene (AN) in helium droplets.<sup>12</sup> Despite the identical symmetry of both molecules, remarkable differences are observed in the helium-induced fine structure of both dopant molecules, which could serve as test spectra for theoretical models simulating microsolvation in superfluid helium droplets.

## II. EXPERIMENT

The experimental setup consists of a two chamber vacuum machine equipped with a pulsed helium droplet source described in Ref. 28. Helium droplets were formed by the expansion of pure helium (6.0 purity) under a stagnation pressure of 80 bars through an Even-Lavie valve modified for cryogenic operation with an orifice of 60  $\mu\text{m}$  in diameter. The valve was attached to a closed cycle cryostat, and cooled to a temperature of 21–22 K producing droplets with an average size of about  $10^5$  He atoms. The valve, which can be operated at a repetition rate of up to 1 kHz, was synchronized to the repetition rate of the laser system limited to 50 Hz. At a distance of 5 cm downstream, the droplet beam passed through a home built conically shaped skimmer of 6 mm diameter, and 13 cm further downstream through a pick-up cell. The pick-up cell was resistively heated to 343 K for sublimating the solid sample. The temperature was adjusted for optimizing single molecule doping of the helium droplets. About 8 cm behind the pick-up unit, the doped droplet beam was crossed perpendicularly by an excimer laser (Lambda Physics LEXTRA 100) (50 Hz) pumped pulsed dye laser (Lambda Physics LPD3000) beam. The band width of the laser was about  $0.2\text{ cm}^{-1}$ . The wavelength of the pulsed dye laser was not calibrated for absolute values. However, as found by comparison with a single mode ring dye laser equipped with a high resolution wavemeter, the pulsed dye laser frequency reading needed an offset of  $-5\text{ cm}^{-1}$  to match the same molecular resonances with an accuracy of  $\pm 1\text{ cm}^{-1}$ . The molecular fluorescence was collected perpendicular to both the droplet beam axis and the laser beam axis and imaged onto the cath-

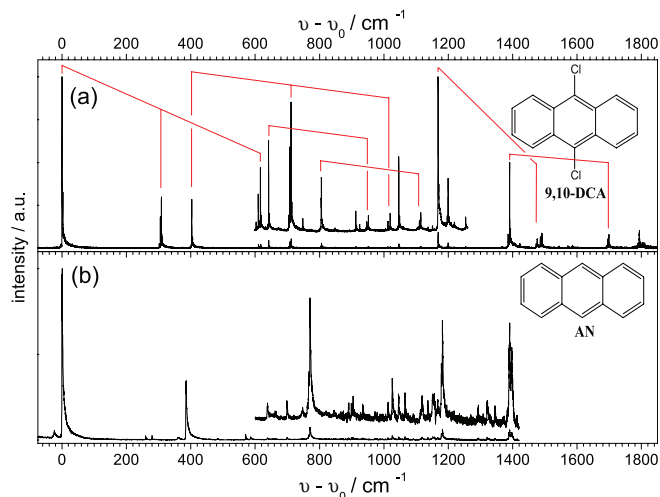


FIG. 1. Fluorescence excitation spectra of 9,10-DCA with  $\nu_0 = 25\,889\text{ cm}^{-1}$  (a) and of AN with  $\nu_0 = 27\,622\text{ cm}^{-1}$ , (b) both in helium droplets and normalized to the laser intensity. The spectra in the inset were recorded with higher laser intensity. At the given laser intensity (below  $10\ \mu\text{J}/\text{pulse}$ ), all excitations were unsaturated. Red combs indicate the progression of the C-Cl stretching mode and the combinations of the progression.

ode of a photomultiplier tube (PMT) (Hamamatsu R943-02). The PMT signal was amplified (Ortec VT120) and fed into a boxcar averager (Scientific Instruments SRS250). Spectra were taken while operating the dye laser in burst mode.<sup>29</sup> For each laser wavelength, the signal was averaged over either 30 (Fig. 1), or 100 (Figs. 2–4) laser pulses. The averaged signal

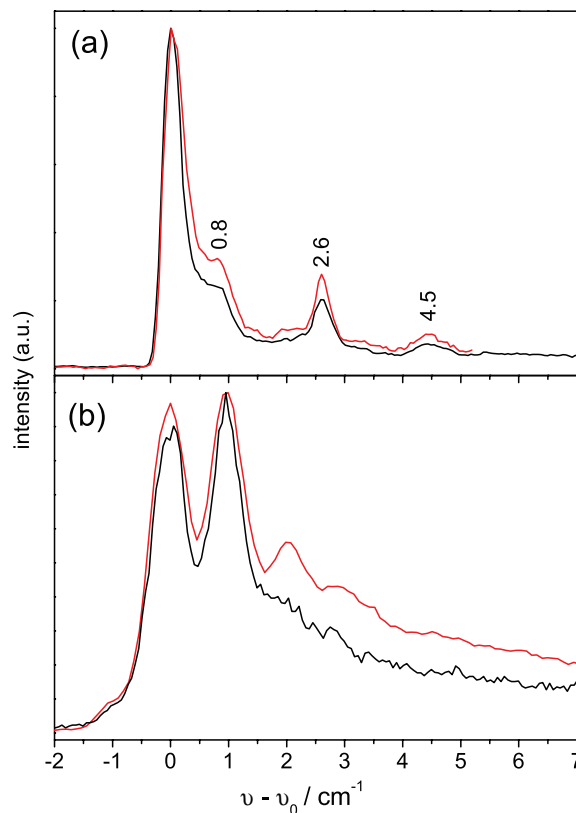


FIG. 2. Fluorescence excitation spectra of 9,10-DCA with  $\nu_0 = 25\,889\text{ cm}^{-1}$  (a) and of AN with  $\nu_0 = 27\,622\text{ cm}^{-1}$  (b) both in helium droplets. A section of  $9\text{ cm}^{-1}$  shows the electronic origin recorded twice, without saturation (black) and with the first peak saturated (red). (see text)

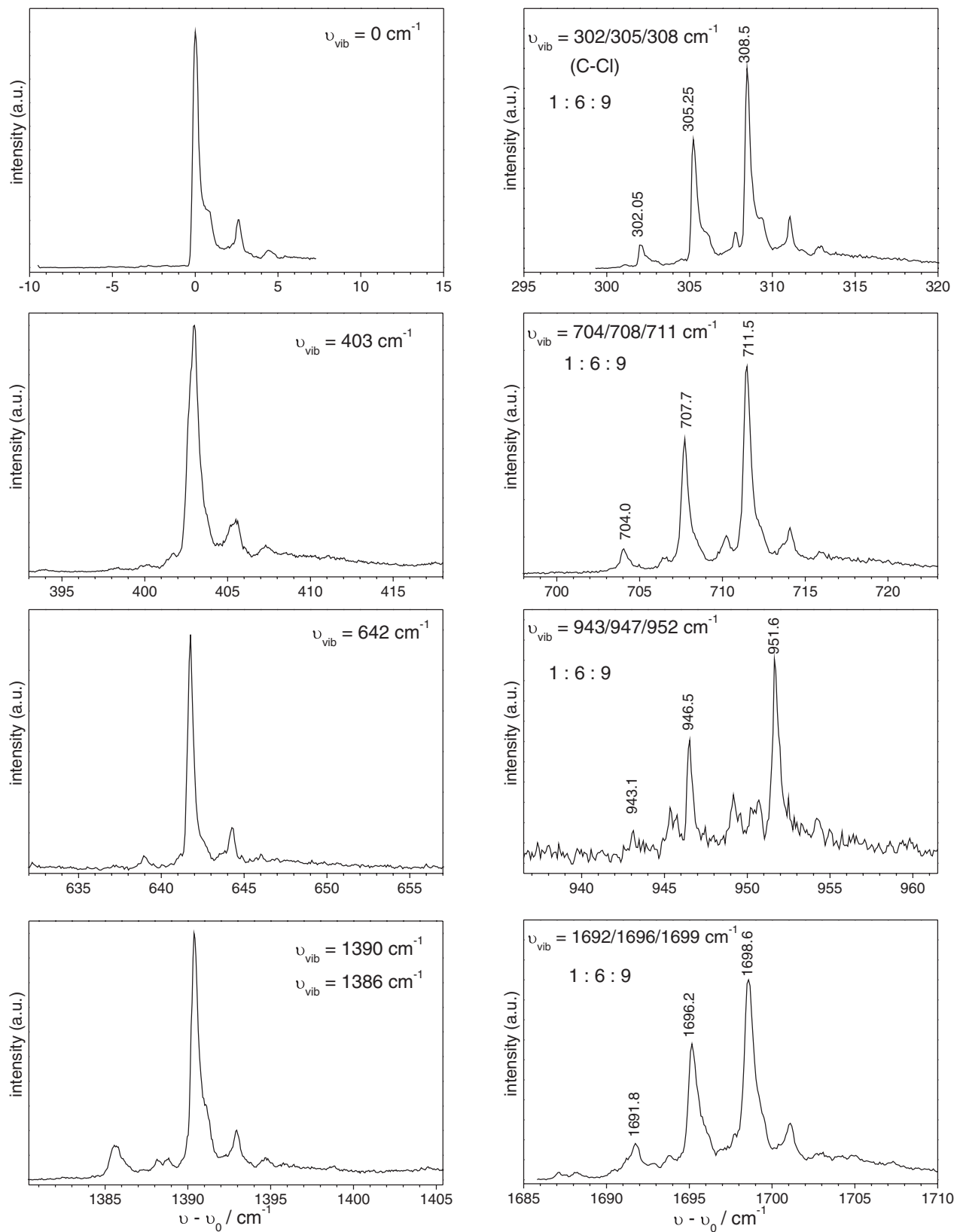


FIG. 3. Fluorescence excitation spectra of selected vibronic bands of 9,10-DCA in helium droplets on an expanded scale. The frequency was scaled to  $\nu_0 = 25\,889 \text{ cm}^{-1}$ . The left column shows the origin (top panel) and three fundamentals with frequencies as indicated. The right column shows the same transitions in combination with the symmetric C-Cl stretching mode.

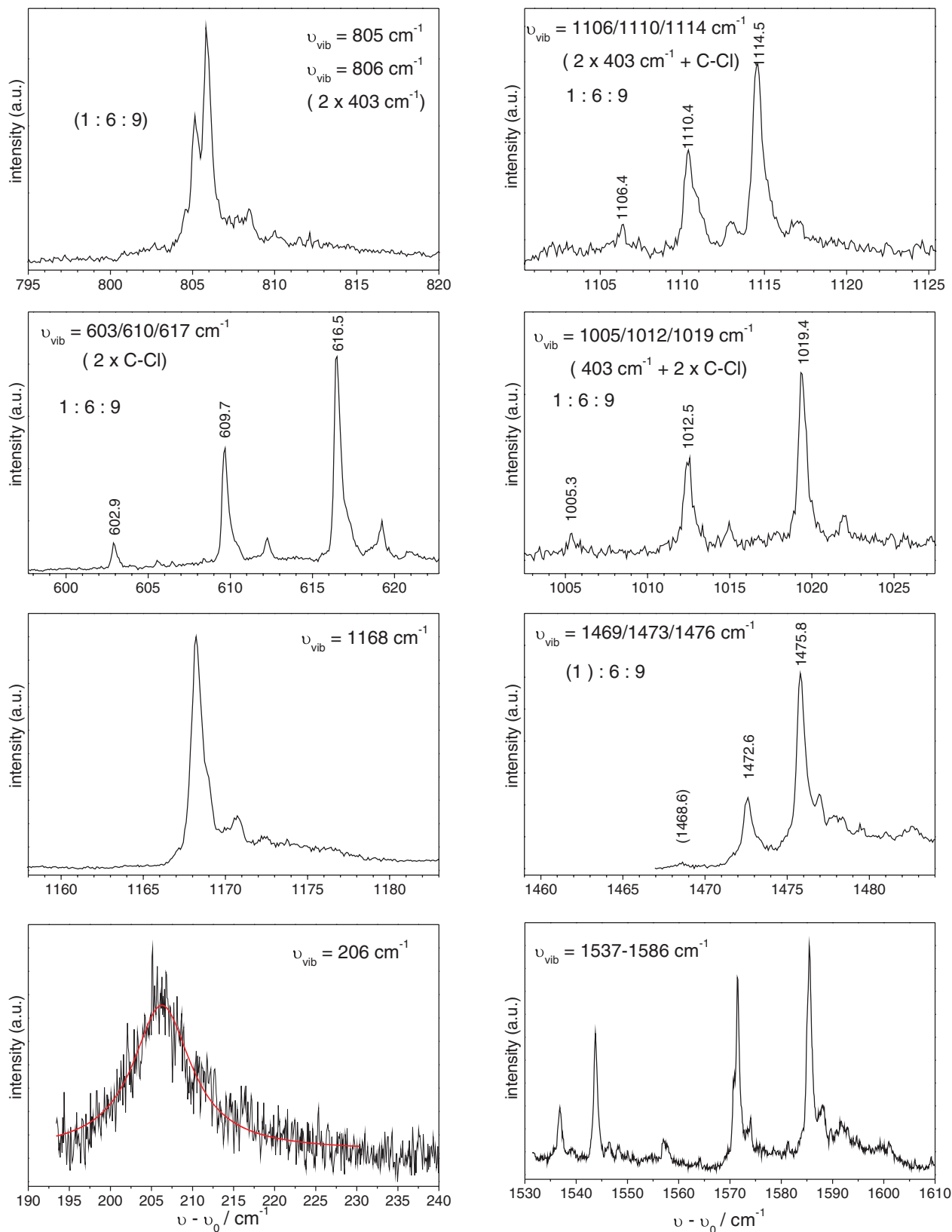


FIG. 4. Fluorescence excitation spectra of selected vibronic bands of 9,10-DCA in helium droplets on an expanded scale. The frequency was scaled to  $\nu_0 = 25\,889\text{ cm}^{-1}$ . Left column shows two first overtones and two additional fundamentals. For the bottom panel, the frequency range is doubled. The right column shows the same vibrational modes in combination with the C-Cl stretching mode except for the bottom panel, which shows a section of  $80\text{ cm}^{-1}$  with vibronic transitions. The line shape of the  $206\text{ cm}^{-1}$  mode was fitted with a Lorentzian (red) with a full width of  $8\text{ cm}^{-1}$ . (see text)

was digitized (Scientific Instruments SRS245), and recorded together with the corresponding laser wavelength. Simultaneously, the laser intensity was recorded in order to eliminate the intensity profile of the dye laser. Laser stray light collected by the imaging optics was minimized by placing an edge filter with a cut-off wavelength of 395 nm (Schott GG 395) in front of the PMT. For dispersed emission spectra, the laser was kept in resonance with a molecular transition and the fluorescence was imaged onto the entrance slit of a spectrograph. The spectrograph consists of a grating spectrometer (LOT Oriol MS257) and a charge coupled device (CCD) camera (ANDOR iDUS). The CCD chip consists of  $256 \times 1024$  pixels and was operated in full vertical binning mode providing spectra with 1024 data points. Emission spectra were frequency calibrated using an Ar/Ne calibration lamp. For the wavelength range of the electronic origin of the  $S_0$ - $S_1$  transition of 9,10-DCA, the spectral resolution was either  $3.9 \text{ cm}^{-1}$ , or  $1.6 \text{ cm}^{-1}$  per CCD pixel for two different gratings, respectively. In the following, the  $3.9 \text{ cm}^{-1}$  and the  $1.6 \text{ cm}^{-1}$  resolution will be addressed as low and high resolution, respectively. The 9,10-DCA was purchased from Aldrich with a purity of at least 96% and was used without further purification. AN data reported in Ref. 31 were recorded using the same experimental setup.

### III. EXPERIMENTAL RESULTS

The fluorescence excitation spectrum of 9,10-DCA in helium droplets is shown in Fig. 1(a) with a frequency axis adjusted to  $\nu_0 = 25\,889 \text{ cm}^{-1}$ . The first transition at the low frequency side is assigned to the electronic origin. As in the gas phase, it is the most intense transition. Due to helium solvation, it is shifted by about  $60 \text{ cm}^{-1}$  to the red.<sup>20</sup> On average, the solvent shift of electronic transitions and of vibrational frequencies for molecules in helium droplets is in the order of  $\pm 1\%$  (for 9,10-DCA cf. Table I). The progression of the  $305 \text{ cm}^{-1}$  mode assigned to the symmetric C-Cl stretching mode and the combination of this progression with other vibrational modes (cf. Refs. 17, and 30) are marked by red line combs in Fig. 1(a). By eliminating all peaks involving the fundamental or overtones of the  $305 \text{ cm}^{-1}$  mode, the remaining transitions reflect very well the frequency pattern of the fluorescence excitation spectrum of bare AN in helium droplets shown in Fig. 1(b).<sup>31</sup> Such similarities are also found in the gas phase as well as in solid matrices.<sup>20,30</sup>

Plotted on a larger scale, the electronic origin in the droplet spectrum reveals a fine structure shown in Fig. 2(a). An intense peak is followed by three much weaker peaks shifted by 0.8, 2.6, and  $4.5 \text{ cm}^{-1}$  to the blue. As shown in Figs. 3 and 4, this pattern repeats at each vibronic transition. Such a feature is entirely absent in the gas phase. Fig. 2(a) shows the electronic origin recorded for two different laser intensities. Both spectra are normalized to the corresponding peak intensity at  $\nu - \nu_0 = 0$ . At laser intensities as used for the black line spectrum and below, the intensity pattern remains constant whereas at higher laser intensities (red line), the relative intensity of the tiny peaks increases with respect to the first peak (at  $\nu - \nu_0 = 0$ ). This is due to saturation of the first peak, which obviously exhibits a larger transition probability.

TABLE I. Relative wavenumbers  $\nu - \nu_0$  ( $\text{cm}^{-1}$ ) in excitation and peak intensities of 9,10-DCA in helium droplets with  $\nu_0 = 25\,889 \text{ cm}^{-1}$ ,  $I_0 = 1$ . Only the leading intense peak of the fine structure is listed (cf. text). For comparison, the most intense transitions of 9,10-DCA in the gas phase  $\nu_{vib}(\text{jet})$  are listed from Ref. 20 without isotope splitting.

$\nu - \nu_0 / \text{cm}^{-1}$ (Droplet)	$I/I_0$ (Droplet)	$\nu_{vib}/\text{cm}^{-1}$ (Jet)	shift/ $\text{cm}^{-1}$ (Droplet)
0	1.000	0	0
206	0.02	198	+8
302	0.03		
305	0.18	306 <sup>a</sup>	$\approx -1$
308	0.28		
398	0.01		
400	0.01		
403	0.28	401	+2
603	0.004		
610	0.022	612 <sup>a</sup>	$\approx -2$
617	0.03		
642	0.05		
705	0.006		
708	0.037	711 <sup>a</sup>	$\approx -3$
712	0.053		
806	0.03	805	+1
913	0.01		
943	<0.001		
947	0.005		
952	0.007		
1005	0.001		
1013	0.008		
1020	0.009		
1047	0.024		
1106	0.001		
1110	0.006		
1115	0.01		
1168	0.09	1168	0
1197	0.01		
1200	0.03		
1254	0.009		
1330	0.004		
1367	0.005		
1386	0.08		
1391	0.50	1390	+1
1422	0.03		
1473	0.03		
1476	0.05	1474	+2
1486	0.07		
1491	0.09	1488	+3
1537	0.005		
1544	0.01		
1572	0.009		
1586	0.015		
1692	0.01		
1696	0.05	1696 <sup>a</sup>	0
1699	0.08		
1794	0.10		

<sup>a</sup>Isotopomers.

<sup>b</sup>Presumably isotopomers.

The spectral position, namely being the first transition at the low frequency side of the spectrum, in combination with the transition probability exceeding the signal to the blue is indicative for a ZPL, while the lower transition probability of the tiny peaks to the blue may speak for a PW. However, the

intensity pattern of the tiny peaks in Fig. 2(a) deviates drastically from what is expected for purely superfluid helium<sup>32</sup> and exhibits surprisingly sharp features indicative for localized helium atoms. For comparison, the electronic origin of bare AN is shown in Fig. 2(b). According to a detailed spectroscopic analysis,<sup>13</sup> the four peaks were assigned to a ZPL while the broad tail extending to the blue with greatly reduced transition probability was assigned to a PW.

An important aspect concerning a fine structure or line splitting in the electronic spectrum of 9,10-DCA are the isotopes of Cl. The natural abundance ratio of the isotopes <sup>37</sup>Cl and <sup>35</sup>Cl amounts to 1:3 and thus the isotopomers (<sup>37</sup>Cl, <sup>37</sup>Cl)-AN, (<sup>35</sup>Cl, <sup>37</sup>Cl)-AN, (<sup>35</sup>Cl, <sup>35</sup>Cl)-AN are expected at an abundance ratio of 1:6:9.<sup>17</sup> For the fine structure shown in Fig. 2(a), the saturation behavior, the intensity pattern, and the number of peaks clearly speak against a Cl isotope effect. However, signals exhibiting the isotope-induced triplet feature with an intensity ratio of 1:6:9 are observed for vibronic transitions, in particular for the symmetric C–Cl stretching mode at 305 cm<sup>-1</sup> and all of its combinations with other modes as shown for several examples in the right column of Figs. 3 and 4. The isotopic shift of the 305 cm<sup>-1</sup> fundamental given by the frequency gap within the triplet feature amounts to 3.2 cm<sup>-1</sup> (cf. top panel right column in Fig. 3) similar as found in the gas phase.<sup>17</sup> As to be expected, the first overtone of the same mode at 610 cm<sup>-1</sup> shows an isotopic splitting with gaps of 6.8 cm<sup>-1</sup> (cf. 2nd panel left column in Fig. 4) about two times larger than for the fundamental. The isotopically induced frequency shift reflects almost perfectly the isotope dependency of the vibrational frequency, which scales inversely to the square root of the reduced mass of the two Cl atoms, a perfect confirmation of the mode assignment. For vibrational fundamental modes at 403, 642, 1168, and 1390 cm<sup>-1</sup> (cf. left column in Figs. 3 and 4) and for the electronic origin, an isotopic splitting is not resolved. Obviously, the two Cl atoms are only marginally involved in these four modes as is confirmed by the appearance of these modes in the AN spectrum. However, in combination with the 305 cm<sup>-1</sup> mode, they all show an isotope splitting very similar to the bare 305 cm<sup>-1</sup> mode (cf. right column in Figs. 3 and 4). Looking at the first overtone of the 403 cm<sup>-1</sup> mode at 805 cm<sup>-1</sup> (cf. top panel left column in Fig. 4), a 1:6:9 intensity pattern is resolved, which reflects twice the isotopic shift of the corresponding fundamental. Although the isotopic shift of the 403 cm<sup>-1</sup> mode could not be resolved, it is still recognizable in the line width, which is larger than at the origin or the 642 cm<sup>-1</sup> or 1390 cm<sup>-1</sup> modes (cf. left column in Fig. 3). It should be noted that all transitions, whether isotopically resolved or not, exhibit the same fine structure as observed at the electronic origin (cf. Figs. 2–4). This observation confirms the assignment of this fine structure to a pure solvent effect and speaks clearly against a Cl isotope effect. Due to the differences in the zero point energy between the electronic ground and excited states for the different isotopomers, the isotopic splitting should also be present at the electronic origin. The experiment does not resolve an isotope splitting at the electronic origin as expected due to the almost identical vibrational frequencies in S<sub>0</sub> and S<sub>1</sub>.

In contrast to all other vibronic transitions of 9,10-DCA and also to the corresponding gas phase spectrum,<sup>20</sup> the low energy mode with a vibrational frequency of 206 cm<sup>-1</sup> shows drastic line broadening (cf. 4th panel left column in Fig. 4). As a consequence, the peak intensity is greatly reduced as can be recognized from the small signal to noise level. At the given sensitivity, the corresponding peak is hardly recognized in the spectrum shown in Fig. 1(a). Nevertheless, upon appropriate averaging, the peak could clearly be recorded and fits perfectly to a Lorentzian of about 8 cm<sup>-1</sup> full width at half maximum. Neither an isotopic splitting, nor the fine structure due to helium solvation can be resolved. A possible explanation for the Lorentzian type line broadening could be substantial damping of the low energy mode by the helium environment. The line width corresponds to a life time of 0.7 ps for the vibronically excited state. For AN, the corresponding mode has a frequency of 209 cm<sup>-1</sup> in the gas phase, and was not observable in helium droplets. Most likely, for both molecules these vibrations represent the first overtone of the butterfly mode. This kind of large amplitude modes are known to be damped by the helium environment.<sup>9,13,14</sup> Vibrational frequencies of 9,10-DCA in the S<sub>1</sub> state as read from the fluorescence excitation spectrum are listed in Table I (first column) together with the peak intensities (second column) normalized to the electronic origin. In addition, some gas phase data are added (third column) together with the corresponding helium solvation shift (last column). In Ref. 17, only the most intense transitions are listed without isotope splitting.

The dispersed emission spectrum of 9,10-DCA upon excitation at the electronic origin recorded at low resolution is shown in Fig. 5(a). The spectrum was transformed to a frequency scale after the calibration of the wavelength axis by means of an Ar-Ne lamp. Thereby, the absolute frequency position was less accurate than the relative frequency position. The frequency at the electronic origin of the spectrum was determined to 25 893 cm<sup>-1</sup> with an uncertainty of ±10 cm<sup>-1</sup>. Within the experimental accuracy, this value matches with the origin in the excitation spectrum. The vibrational frequencies in S<sub>0</sub> read from the emission spectra are listed in Table II (first column) together with the peak intensities (second column) normalized to the electronic origin. As can be seen from the last two columns of Table II, the vibrational frequencies match well with the corresponding gas phase data recorded upon excitation at the electronic origin.<sup>20,21</sup> Remarkable similarities are also found for the vibrational frequencies in the S<sub>0</sub> and S<sub>1</sub> state of 9,10-DCA (cf. Tables I and II) as to be expected for a rigid molecule. Most of the vibrational structure in the emission spectrum of 9,10-DCA is also observed in the emission spectrum of AN. Additional peaks reflect fundamentals and overtones of the C-Cl stretching which appear also coupled to other vibrational modes (cf. Figs. 5(a) and 5(b)). The large values for the shift listed in the last column of Table II are due to the spectral resolution and frequency calibration, which is much lower and less accurate for dispersed emission than for fluorescence excitation. As for AN, the mirror symmetry of excitation and emission spectra breaks down for vibrational energies beyond about 800 cm<sup>-1</sup>. The same is observed in the supersonic jet (for emission spectra recorded

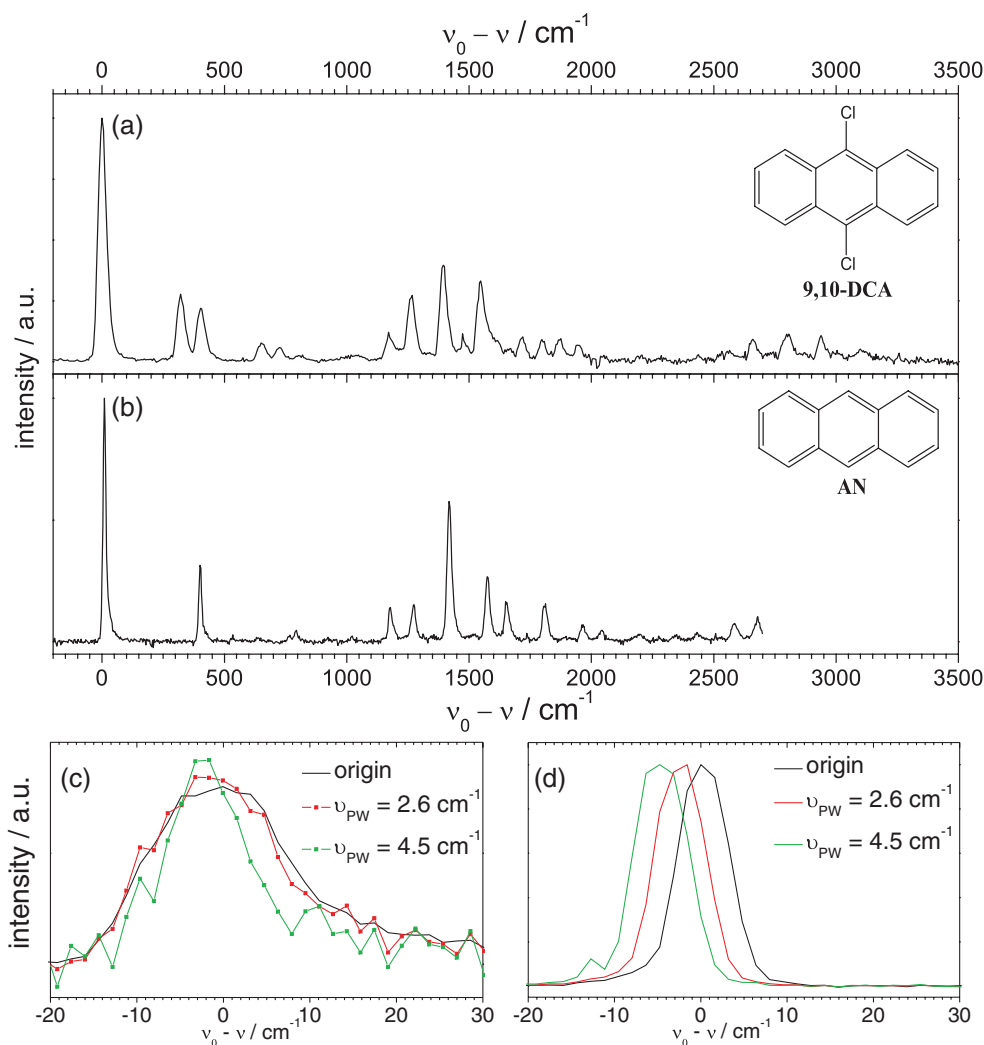


FIG. 5. Low resolution dispersed emission spectra of 9,10-DCA with  $\nu_0 = 25\,893\text{ cm}^{-1}$  (a) and of AN with  $\nu_0 = 27\,622\text{ cm}^{-1}$  (b) both in helium droplets. Three high resolution dispersed emission spectra of 9,10-DCA (c) recorded upon excitation as indicated and of the laser stray light (d) for the three excitation frequencies. The frequency axis was adjusted to  $\nu_0 = 25\,893\text{ cm}^{-1}$ .

upon excitation at the electronic origin), which was attributed to Fermi-resonance effects.<sup>20</sup>

In contrast to the supersonic jet, emission spectra recorded in helium droplets are independent of the excitation frequency. Obviously, in spite of different vibronic excitation, the emission originates always from the same level. This level is identified as the vibrational ground level of  $S_1$  by the matching frequencies of the origin in the fluorescence excitation spectrum with those of all emission spectra. As reported for numerous molecules, also for anthracene derivatives the excess excitation energy is dissipated into the droplet prior to radiative decay. Fast dissipation of excess excitation energy beyond the electronic origin is well known for matrix isolation spectroscopy, and has been demonstrated in helium droplets most detailed for phthalocyanine with excess energies of up to  $12\,900\text{ cm}^{-1}$ .<sup>38</sup> It has been confirmed for excess excitation energies up to  $1600\text{ cm}^{-1}$ .<sup>9</sup>

As outlined above, dispersed emission spectra are an important source of information to analyze spectral features observed in the fluorescence excitation spectrum, in particular of those features reflecting microsolvation. If the dispersed

emission carries radiation which coincides with the excitation frequency, the corresponding excitation marks the ZPL at the electronic origin. All other transitions of the same dopant species carry excess excitation energy either intramolecular deposited into nuclear or electronic degrees of freedom, or intermolecular deposited into the excitation of the helium environment, or both. Among these three cases, intramolecular excess excitation is a pure molecular excitation and therefore a ZPL. The other two cases include excitation of the helium environment, and are therefore assigned as PW. The dispersed emission spectra cannot discriminate between these cases. However, the transition probability of a ZPL exceeds that of a PW, which can be deduced from the corresponding saturation behavior. In the case of a single dopant species, all transitions in the excitation spectrum show the same dispersed emission spectrum as obtained upon excitation at the ZPL of the electronic origin. Consequently, the number of transitions which show emission coincident with its own excitation frequency corresponds to the number of electronic origins and, thus, of different dopant species. This experimental procedure is well known from matrix isolation spectroscopy to

TABLE II. Relative wavenumbers  $\nu_0 - \nu$  ( $\text{cm}^{-1}$ ) in the emission spectrum of 9,10-DCA in helium droplets with  $\nu_0 = 25\,893\text{ cm}^{-1}$  and their relative intensities  $I/I_0$ . For comparison, vibrational frequencies in the ground state of 9,10-DCA observed in the gas phase,<sup>21</sup>  $\nu_{vib}(\text{jet})$ , are listed.

$\nu_0 - \nu / \text{cm}^{-1}$ (Droplet)	$I/I_0$ (Droplet)	$\nu_{vib} / \text{cm}^{-1}$ (Jet)	shift / $\text{cm}^{-1}$ (Droplet)
0	1.00	0	0
321	0.28	306,309	+15,+12
403	0.22	403	0
653	0.08	641	+12
728	0.06	707,710	+21,+18,
809	0.03	805	+4
1031	0.02	1045	-14
1171	0.12	1169	+2
1263	0.26	A <sup>a</sup>	...
1394	0.40	1390	+4
1473	0.12	1489	-16
1548	0.33	1582	-34
1612	0.09	...	...
1715	0.10	1696	+19
1802	0.08	1792	+10
1870	0.09	...	...
1946	0.07	...	...
2660	0.09	...	...
2802	0.11	...	...
2938	0.11	...	...

<sup>a</sup>A is the intense  $1263\text{ cm}^{-1}$  vibration in the droplet spectrum not listed in Ref. 21, but clearly visible in their spectrum.

distinguish identical dopant molecules differently embedded into the matrix (addressed as sites). It has been applied to identify different species such as the  $\alpha$  and  $\beta$  version of tetracene, solvation complexes of AN (both in Ref. 31), and isomeric configurations of phthalocyanine-Ar clusters.<sup>27</sup> In order to further analyze the fine structure at the electronic origin of 9,10-DCA, this procedure was applied as previously done for AN. Thus, emission spectra were recorded upon excitation at the three most prominent peaks resolved in Fig. 2(a). In order to compare the emission spectra recorded upon excitation at  $0\text{ cm}^{-1}$  (black),  $2.6\text{ cm}^{-1}$  (red), and  $4.5\text{ cm}^{-1}$  (green), a section of  $50\text{ cm}^{-1}$  of the corresponding emission spectra showing only the first peak at the high frequency side are plotted in Fig. 5(c) for an identical frequency scale adjusted to  $25\,893\text{ cm}^{-1}$ . The width of the three peaks exceeds the shift of the excitation frequencies by far. However, the shift of the peak positions of the three spectra is less than a single pixel of the CCD camera whereas the shift of the excitation frequency amounts to about 1.5 CCD pixel as revealed by the bare laser stray light measured consecutively for all three excitation frequencies (cf Fig. 5(d)). Therefore, we conclude the spectral coincidence of all three emission spectra and in addition with the most prominent line at the electronic origin for all three emission spectra. Consequently, the first line at  $0\text{ cm}^{-1}$  represents the ZPL at the electronic origin. The excess excitation energy of  $2.6\text{ cm}^{-1}$  and  $4.5\text{ cm}^{-1}$  dissipates prior to radiative decay. Since this excess excitation energy does not fit to intramolecular modes and in view of the saturation behavior revealing reduced transition probability, these resonances are assigned to a PW.

## IV. DISCUSSION

The electronic spectra of 9,10-DCA in helium droplets reveal rather gentle perturbations of the dopant molecule by the helium environment. Except for the low energy mode at  $206\text{ cm}^{-1}$ , the vibrational frequencies and the electronic transition energy are altered by less than 1% compared to the gas phase. In this respect, 9,10-DCA behaves identical as AN (cf. Ref. 31). The most pronounced spectral feature reflecting solvation in helium droplets is the fine structure shown in Fig. 2(a) for the electronic origin. The fine structure reappears identically for each vibronic transition (cf. Figs. 3 and 4). Also for AN, a fine structure was resolved, which reappears identically for all transitions in the excitation spectrum, however, of entirely different shape than in the case of 9,10-DCA (Fig. 2). According to the different saturation behavior and the spectral coincidence of the emission spectra upon selective excitation both within the fine structure, we assign the first peak at the low frequency side to the ZPL and the three peaks following to the blue to a PW. The coincident emission spectra could also reveal the presence of various metastable configurations of a dopant-helium solvation complex, which upon electronic excitation, undergo relaxation into the global minimum configuration prior to radiation. However, it is rather unlikely that a modification of the configuration of a certain number of weakly interacting helium atoms should cause significant differences in the transition probability for electronic excitation, as observed within the fine structure. Therefore, the experimental data favor the assignment to a singly peaked ZPL accompanied by a sharply structured PW. Without the additional information gained from dispersed emission spectra and from the saturation behavior, an assignment of peaks within the fine structure is questionable. The simple classification of sharp peaks as ZPL, and of broader features as PW, is inappropriate. With respect to the study of microsolvation fluorescence detection thus outmatches the depletion method, since depletion records only absorption and in most cases even under severe saturation.

Microsolvation in superfluid helium droplets is revealed by spectral features such as multiplet splitting of the ZPL and the spectral structure of the PW. Up to now, a theoretical model to simulate or even predict spectral features of the solvation in helium droplets quantitatively is not available (cf. chapter 5 in Ref. 9). Empirical explanations are readily on hand. Configurational modifications of the closer host-guest environment, which corresponds to *sites* in matrix isolation spectroscopy, rationalize the phenomenon of multiplet splitting of the ZPL. A sharply structured PW is in contrast to the well-known phonon spectrum of superfluid helium.<sup>32</sup> Sharp peaks in the PW reveal individual helium atoms localized at the surface of the dopant molecule, which by definition are non-superfluid. The challenge to be accepted is to calculate not only the appropriate dopant- $\text{He}_n$  complex, but in addition its spectroscopic response when inside a superfluid helium droplet. So far, few individual molecules have been considered to develop theoretical models for microsolvation. We aim to shed light on microsolvation in helium droplets by comparing data for a set of related dopant species, in the present case different anthracene derivatives. At this point, we have

compared the electronic spectra of AN as published in Ref. 31 with those of 9,10-DCA. The variation in the spectral shape of the ZPL and the PW presented in Fig. 2 is remarkable. Both anthracene compounds exhibit the same molecular symmetry while they differ in the mass and the electron density distribution. Since the fine structure shown in Fig. 2 is identical for all vibronic transitions, it appears to be rather independent of nuclear conditions. Therefore, we conclude the electronic density distribution to be responsible for the shape of the fine structure and thus for what is called microsolvation. This concept parallels to the configuration coordinate model discussed for matrix isolation spectroscopy.<sup>33-35</sup> As outlined in an extensive investigation of various organic molecules in helium droplets,<sup>13</sup> the anthracene derivatives confirm that electronic spectroscopy in helium droplets appears to be highly sensitive to changes of the electron density distribution. We believe that high quality interaction potentials are mandatory for the simulation of the spectral fine structure of electronic transitions of molecules in superfluid helium droplets.

Besides the fine structure, the intensity distribution within the electronic excitation spectrum reveals information on the dopant to helium interaction. The intensity pattern of an absorption spectrum depends on the absorption cross section while that of an fluorescence excitation spectrum is additionally weighted by the fluorescence quantum yield as shown in Eq. (1).

$$I^{LIF}(v) \propto \underbrace{|\langle \Psi_{a0} | \hat{\mu} | \Psi_{b\beta} \rangle|^2}_{\text{absorption}} \Phi_{b\beta}^r. \quad (1)$$

Both factors in Eq. (1) depend on the excited level denoted by the indices  $b$  and  $\beta$  as the electronic and vibrational excitation, respectively. The fluorescence quantum yield  $\Phi_{b\beta}^r$  thereby describes the probability that the decay of a particular excited state ( $\Psi_{b\beta}$ ) contributes to photon emission within the time of the measurement.<sup>20,36,37</sup> This may include the direct radiative decay as well as secondary radiation preceded by internal conversion (IC), internal vibrational redistribution (IVR), or inter-system crossing (ISC). Fluorescence excitation and absorption spectra measured for 9,10-DCA in a supersonic jet as reported in Ref. 20 are shown in Figs. 6(b) and 6(c), respectively. Both spectra show similar intensities at the low frequency side while for increasing frequency, the signal in the fluorescence spectrum decreases as compared to the absorption. This can exemplarily be recognized for the vibronic transitions at 401 and 1390  $\text{cm}^{-1}$ . The discrepancy of the intensities of the two spectra reveals a state specific fluorescence quantum yield plotted on a logarithmic scale in panel (a). The decrease of the fluorescence quantum yield with increasing vibrational energy was ascribed to an increase of the non radiative ISC-rate mediated via IVR.<sup>20</sup>

A comparison with the fluorescence excitation spectrum of 9,10-DCA in helium droplets (Fig. 6(d)) reveals a remarkable similarity to the gas phase absorption spectrum (c). Obviously, in helium droplets the state specificity of the fluorescence quantum yield is vanished. As discussed above, in helium droplets an additional fluorescent decay channel is opened by the dissipative environment. The corresponding fluorescence quantum yield is given by the quantum

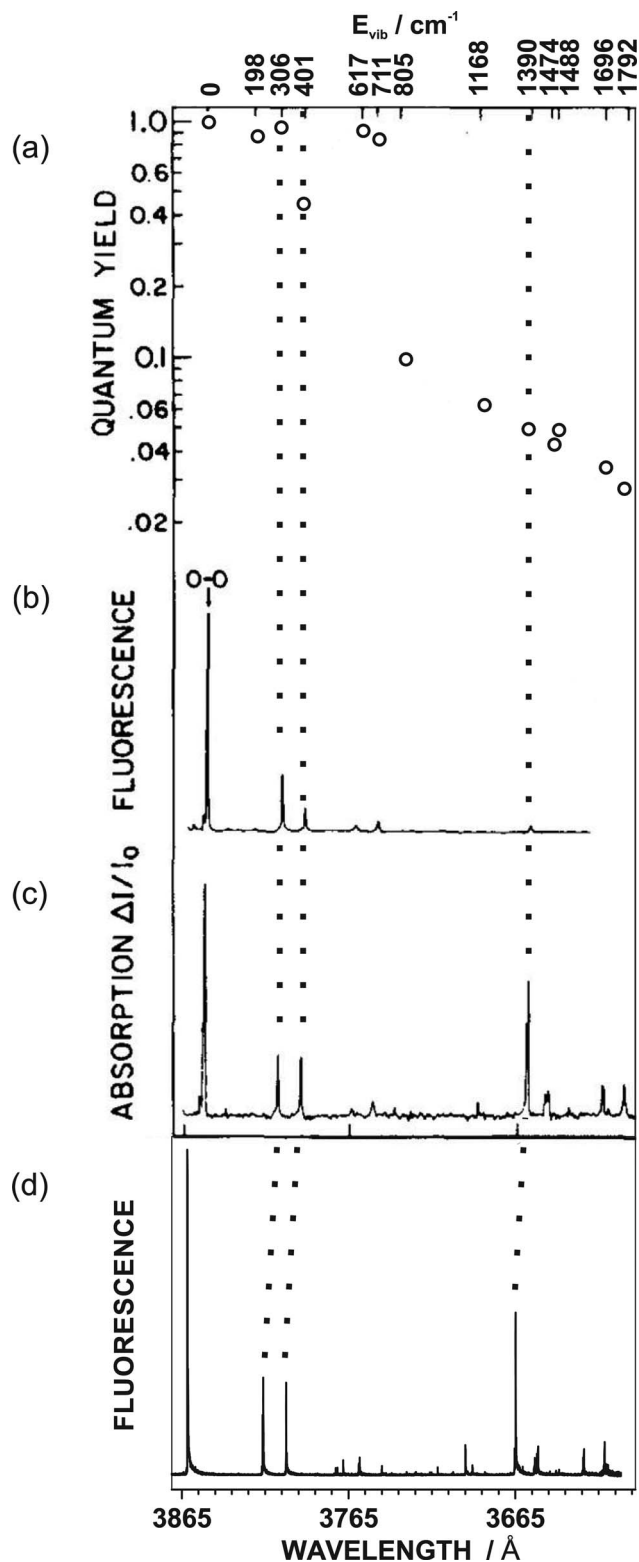


FIG. 6. Fluorescence quantum yield (a) of 9,10-DCA in a supersonic jet as deduced from the simultaneous measurement of the fluorescence excitation spectrum (b) and the absorption spectrum (c). Bottom panel shows the fluorescence excitation spectrum of 9,10-DCA recorded in helium droplets (d). Gas phase data are taken from Ref. 20.

yield for relaxation of the excited level ( $\Psi_{b\beta}$ ) into the vibrational ground level of  $S_1$  ( $\Psi_{b0}$ ) via energy dissipation,  $\Phi_{b\beta}^{diss}$ , weighted by the fluorescence quantum yield of the ground level of  $S_1$ ,  $\Phi_{b0}^r$ . Thus, the fluorescence quantum yield in

helium droplets is given by the sum of this helium induced contribution and the intramolecular contribution discussed in Eq. (1) possibly modified by the droplet environment as indicated by the additional upper index ( $\Phi_{b\beta}^{r,droplet}$ ).

$$\Phi_{b\beta}^r = \Phi_{b\beta}^{r,droplet} + \Phi_{b\beta}^{diss} \cdot \Phi_{b0}^r \approx \Phi_{b\beta}^{diss} \cdot \Phi_{b0}^r. \quad (2)$$

Dispersed emission spectra in helium droplets show that fluorescence originates exclusively from the ground level of  $S_1$ .<sup>7,25,26,31,38–40</sup> Thus, the intramolecular contributions to fluorescence,  $\Phi_{b\beta}^{r,droplet}$ , can be neglected.  $\Phi_{b\beta}^{diss}$  may depend on the excited state  $\Psi_{b\beta}$  since the relaxation into the vibrational ground state of  $S_1$  may compete with other processes such as relaxation into possible dark states or into the electronic ground state or long lived triplet states. However, the identical intensity pattern for the helium droplet spectrum (cf. Fig. 6(d)) and the absorption spectrum in the gas phase (Fig. 6(c)) reveals a dissipation quantum yield  $\Phi_{b\beta}^{diss}$  of one, independent of  $\beta$ . Hence, the  $\beta$  dependent influence of ISC on the fluorescence quantum yield (cf. Fig. 6(a)) can be excluded in helium droplets.<sup>41</sup> Our data do not allow for providing absolute values for the fluorescence quantum yield in helium droplets.

Finally, some comments are needed on the mechanistic details of the energy dissipation from the excited molecule into the helium droplet. The energy dissipation requires a coupling between the molecular vibration and the phonons of the helium environment. For a direct decay into the emissive state, the line width of the vibronic transitions reflecting the inverse of the life time of the excited level is expected to correlate with the vibrational energy. However, neither for anthracene derivatives (this work,<sup>12,13,31</sup>) nor for phthalocyanine<sup>13</sup> any such correlation has been observed. Therefore, we assume a step-wise decay mechanism, which may involve IVR feeding highly excited low energy modes followed by energy dissipation into the helium droplet. Thus, the homogeneous line width of the vibronic transitions does not reflect the efficiency of the energy dissipation into the helium environment but the efficiency of IVR. As an exception, the large line width of the 206  $\text{cm}^{-1}$  mode may provide evidence for direct coupling to the helium environment.

## V. CONCLUSION

The 9,10-DCA molecule doped into superfluid helium droplets has been investigated by means of electronic spectroscopy. In comparison to gas phase data, the intramolecular energetic conditions in helium droplets were almost identical. The most pronounced signature of the helium environment as revealed by the fluorescence excitation spectrum was a fine structure to which the electronic origin and all vibrational transitions split up. By means of the combined investigation of fluorescence excitation and dispersed emission spectra in addition with the saturation behavior, the fine structure could be assigned to a single peaked ZPL accompanied by a sharply structured PW. The spectral shape of the PW, which deviates drastically from the PW of superfluid helium,<sup>32</sup> provides a clear evidence for a non-superfluid helium solvation layer surrounding the dopant molecule. The spectral shape of the

fine structure comprises a very high specificity for the dopant species as can be recognized by comparison with the corresponding fine structure measured for AN in helium droplets.<sup>31</sup> In contrast to the remarkable response to the symmetry conserving substitution of two hydrogen atoms by chlorine atoms (cf. Fig. 2), the fine structure was identical for all three chlorine isotopes of 9,10-DCA (cf. Figs. 3 and 4). Thus, our result provides further evidence for the electron density distribution playing a key role for microsolvation in superfluid helium.

The dynamics following electronic excitation is revealed by the combined investigation of fluorescence excitation and dispersed emission spectra. As for all dopant molecules investigated by these means, also for 9,10-DCA, the primary step in the decay of vibronically excited levels is the dissipation of excitation energy in excess to the ground level of  $S_1$  into the helium environment possibly mediated by IVR. It holds for the excess energy put into intramolecular as well as intermolecular degrees of freedom and the corresponding quantum yield exceeds that of all intramolecular channels by far. The missing correlation between the homogeneous line width and the vibrational excitation energy in the fluorescence excitation spectrum provides evidence for a step-wise dissipation into the helium droplet. In contrast, the exorbitant width of 8  $\text{cm}^{-1}$  obtained for a Lorentzian fit to the 206  $\text{cm}^{-1}$  mode may be indicative for the direct dissipation of the vibrational energy. For 9,10-DCA, the helium induced decay path of the electronically excited molecule eliminates the loss of fluorescence caused by dark intramolecular decay paths. An optimized fluorescence quantum yield can be expected for any molecule exhibiting a maximum of the fluorescence quantum yield at the electronic origin. This mechanism makes the helium droplets not only attractive for the study of highly excited vibrational levels in  $S_1$ , but possibly also for higher electronic states, which often exhibit only a low fluorescence quantum yield in the gas phase. On the other hand, the decay mechanism of electronically excited states serves as an energy sink and, thus, may significantly influence molecular dynamics as present in reactive processes whether uni-molecular or bimolecular.

Despite the detailed experimental analysis of the fine structure revealing solvation in helium droplets, we are far from a general model explaining and predicting the spectroscopic signature of microsolvation in helium droplets. However, we are confident that the increasing amount of experimental data, especially on structurally similar molecules such as 9,10-DCA and AN, may help to solve this challenging problem. Once this is solved, the fine structure due to helium solvation may serve as a very efficient sensor to monitor changes of the electron density distribution upon electronic excitation of molecules.

<sup>1</sup>J. P. Toennies and A. F. Vilesov, *Annu. Rev. Phys. Chem.* **49**, 1 (1998).

<sup>2</sup>J. P. Toennies and A. F. Vilesov, *Angew. Chem., Int. Ed.* **43**, 2622 (2004).

<sup>3</sup>M. Y. Choi, G. E. Douberly, T. M. Falconer, W. K. Lewis, C. M. Lindsay, J. M. Merritt, P. L. Stiles, and R. E. Miller, *Int. Rev. Phys. Chem.* **25**, 15 (2006).

<sup>4</sup>J. Küpper and J. M. Merritt, *Int. Rev. Phys. Chem.* **26**, 249 (2007).

<sup>5</sup>F. Stienkemeier and K. K. Lehmann, *J. Phys. B* **39**, R127 (2006).

<sup>6</sup>J. Tiggesbäumker and F. Stienkemeier, *Phys. Chem. Chem. Phys.* **9**, 4748 (2007).

- <sup>7</sup>A. Slenczka and J. P. Toennies, "Chemical dynamics inside superfluid helium nanodroplets at 0.37 K," in *Low Temperatures and Cold Molecules*, edited by I. A. M. Smith (World Scientific, Singapore, 2008), p. 345.
- <sup>8</sup>A. Hernando, M. Barranco, M. Pi, E. Loginov, M. Langlet, and M. Drabbels, *Phys. Chem. Chem. Phys.* **14**, 3996 (2012).
- <sup>9</sup>C. Callegari and W. E. Ernst, "Helium droplets as nanocryostats for molecular spectroscopy from the vacuum ultraviolet to the microwave regime," in *Handbook of High-Resolution Spectroscopy*, edited by M. Quack and F. Merkt (Wiley, 2011), p. 1569.
- <sup>10</sup>K. von Haefen, A. Metzethin, S. Rudolph, V. Staemmler, and M. Havenith, *Phys. Rev. Lett.* **95**, 215301 (2005).
- <sup>11</sup>M. Ortlieb, Ö. Birer, M. Letzner, G. Schwaab, and M. Havenith, *J. Phys. Chem. A* **111**, 12192 (2007).
- <sup>12</sup>D. Pentlehner, C. Greil, B. Dick, and A. Slenczka, *J. Chem. Phys.* **133**, 114505 (2010).
- <sup>13</sup>D. Pentlehner, R. Riechers, A. Vdovin, G. M. Pötzl, and A. Slenczka, *J. Phys. Chem. A* **115**, 7034 (2011).
- <sup>14</sup>M. Hartmann, A. Lindinger, J. P. Toennies, and A. F. Vilesov, *J. Phys. Chem. A* **105**, 6369 (2001).
- <sup>15</sup>F. Stienkemeier, J. Higgins, W. E. Ernst, and G. Scoles, *Phys. Rev. Lett.* **74**, 3592 (1995).
- <sup>16</sup>V. Hizhnyakov, I. Tehver, and G. Benedek, *Eur. Phys. J. B* **70**, 507 (2009).
- <sup>17</sup>A. Amirav, U. Even, and J. Jortner, *Anal. Chem.* **54**, 1666 (1982).
- <sup>18</sup>A. Amirav and J. Jortner, *Chem. Phys. Lett.* **94**, 545 (1983).
- <sup>19</sup>A. Amirav, M. Sonnenschein, and J. Jortner, *Chem. Phys.* **88**, 199 (1984).
- <sup>20</sup>A. Amirav, C. Horwitz, and J. Jortner, *J. Chem. Phys.* **88**, 3092 (1988).
- <sup>21</sup>F. Tanaka, S. Yamashita, S. Hirayama, A. Adach, and K. Shobatake, *Chem. Phys.* **131**, 435 (1989).
- <sup>22</sup>A. Penner, A. Amirav, J. Jortner, and A. Nitzan, *J. Chem. Phys.* **93**, 147 (1990).
- <sup>23</sup>N. Ben-Horin, D. Barhatt, U. Even, and J. Jortner, *J. Chem. Phys.* **97**, 6011 (1992).
- <sup>24</sup>A. Penner and A. Amirav, *J. Chem. Phys.* **99**, 9616 (1993).
- <sup>25</sup>R. Lehnig and A. Slenczka, *J. Chem. Phys.* **118**, 8256 (2003).
- <sup>26</sup>R. Lehnig and A. Slenczka, *J. Chem. Phys.* **122**, 244317 (2005).
- <sup>27</sup>R. Lehnig, J. A. Sebree, and A. Slenczka, *J. Phys. Chem. A* **111**, 7576 (2007).
- <sup>28</sup>D. Pentlehner, R. Riechers, B. Dick, A. Slenczka, U. Even, N. Lavie, R. Brown, and K. Luria, *Rev. Sci. Instrum.* **80**, 043302 (2009).
- <sup>29</sup>"Burst Mode" means keeping the laser wavelength fixed while acquiring signal. Subsequently, the laser is tuned by a defined wavelength step and signal acquisition is repeated. Thus, frequency tuning and data acquisition are perfectly synchronized.
- <sup>30</sup>T. P. Carter and G. D. Gillispie, *J. Phys. Chem.* **86**, 2691 (1982).
- <sup>31</sup>D. Pentlehner and A. Slenczka, *Mol. Phys.* **110**, 1933 (2012).
- <sup>32</sup>M. Hartmann, F. Mielke, J. P. Toennies, A. F. Vilesov, and G. Benedek, *Phys. Rev. Lett.* **76**, 4560 (1996).
- <sup>33</sup>I. S. Osad'ko, R. I. Personov, and E. V. Shpol'skii, *J. Lumin.* **6**, 369 (1973).
- <sup>34</sup>J. Friedrich and D. Haarer, *Angew. Chem., Int. Ed.* **23**, 113 (1984).
- <sup>35</sup>K. Rebane, "Zero-phonon lines in the spectroscopy and photochemistry of impurity-doped solid matter," in *Zero-Phonon Lines and Spectral Hole Burning in Spectroscopy and Photochemistry*, edited by O. Solid and K. Haller (Springer, Berlin, 1988), pp. 1–19.
- <sup>36</sup>W. R. Lambert, P. M. Felker, J. A. Syage, and A. H. Zewail, *J. Chem. Phys.* **81**, 2195 (1984).
- <sup>37</sup>M. Klessinger and J. Michl, *Excited States and Photochemistry of Organic Molecules* (VCH, 1995).
- <sup>38</sup>R. Lehnig and A. Slenczka, *J. Chem. Phys.* **120**, 5064 (2004).
- <sup>39</sup>R. Lehnig and A. Slenczka, *Chem. Phys. Chem.* **5**, 1014 (2004).
- <sup>40</sup>A. Stromeck-Faderl, D. Pentlehner, U. Kensy, and B. Dick, *Chem. Phys. Chem.* **12**, 1969 (2011).
- <sup>41</sup>We note, that  $\Phi_{b0}'$  of 9,10-DCA was found to be 1 in the gas phase,<sup>20</sup> which, however, may be different in the droplet due to solvent effects and dissipation of electronic excitation energy.